N-Methyl-D-Aspartate Receptor Hypofunction in Meg-01 Cells Reveals a Role for Intracellular Calcium Homeostasis in Balancing Megakaryocytic-Erythroid Differentiation

James I. Hearn[1] Taryn N. Green[1] Martin Chopra[1] Yohanes N. S. Nursalim[1] Leandro Ladvanszky[1] Nicholas Knowlton[1] Cherie Blenkiron[1] Raewyn C. Poulsen[2,3] Dean C. Singleton[4] Stefan K. Bohlander[1] Maggie L. Kalev-Zylinska[1,5]

[1] Department of Molecular Medicine and Pathology, School of Medical Sciences, University of Auckland, Auckland, New Zealand
[2] Department of Medicine, School of Medicine, University of Auckland, Auckland, New Zealand
[3] Department of Pharmacology and Clinical Pharmacology, School of Medical Sciences, University of Auckland, Auckland, New Zealand
[4] Auckland Cancer Society Research Centre, University of Auckland, Auckland, New Zealand
[5] LabPlus Haematology, Auckland City Hospital, Auckland, New Zealand

Address for correspondence Maggie L. Kalev-Zylinska, MD, PhD, FRCPA, Department of Molecular Medicine and Pathology, University of Auckland, 85 Park Road, Grafton, Private Bag 92019, Auckland, New Zealand (e-mail: m.kalev@auckland.ac.nz).

Thromb Haemost 2020;120:671–686.

Abstract

The release of calcium ions (Ca^{2+}) from the endoplasmic reticulum (ER) and related store-operated calcium entry (SOCE) regulate maturation of normal megakaryocytes. The *N*-methyl-D-aspartate (NMDA) receptor (NMDAR) provides an additional mechanism for Ca^{2+} influx in megakaryocytic cells, but its role remains unclear. We created a model of NMDAR hypofunction in Meg-01 cells using CRISPR-Cas9 mediated knockout of the *GRIN1* gene, which encodes an obligate, GluN1 subunit of the NMDAR. We found that compared with unmodified Meg-01 cells, Meg-01-*GRIN1*$^{-/-}$ cells underwent atypical differentiation biased toward erythropoiesis, associated with increased basal ER stress and cell death. Resting cytoplasmic Ca^{2+} levels were higher in Meg-01-*GRIN1*$^{-/-}$ cells, but ER Ca^{2+} release and SOCE were lower after activation. Lysosome-related organelles accumulated including immature dense granules that may have contributed an alternative source of intracellular Ca^{2+}. Microarray analysis revealed that Meg-01-*GRIN1*$^{-/-}$ cells had deregulated expression of transcripts involved in Ca^{2+} metabolism, together with a shift in the pattern of hematopoietic transcription factors toward erythropoiesis. In keeping with the observed pro-cell death phenotype induced by *GRIN1* deletion, memantine (NMDAR inhibitor) increased cytotoxic effects of cytarabine in unmodified Meg-01 cells. In conclusion, NMDARs comprise an integral component of the Ca^{2+} regulatory network in Meg-01 cells that help balance ER stress and megakaryocytic-erythroid differentiation. We also provide the first evidence that megakaryocytic NMDARs regulate biogenesis of lysosome-related organelles, including dense granules. Our results argue that intracellular Ca^{2+} homeostasis may be more important for normal megakaryocytic and erythroid differentiation than currently recognized; thus, modulation may offer therapeutic opportunities.

Keywords

- *N*-methyl-D-aspartate receptor
- endoplasmic reticulum stress
- intracellular calcium
- megakaryocyte
- erythropoiesis

received
September 21, 2019
accepted
February 4, 2020

DOI https://doi.org/10.1055/s-0040-1708483.
ISSN 0340-6245.

Introduction

Calcium (Ca^{2+}) is an ubiquitous but versatile cytosolic second messenger, oscillations of which regulate gene transcription, including in megakaryocytes (MKs).[1,2] Resting cells maintain cytosolic Ca^{2+} concentrations at very low levels to inhibit apoptosis. This is achieved through the transport of cytosolic Ca^{2+} into the extracellular space or sequestration of Ca^{2+} into intracellular stores, of which endoplasmic reticulum (ER) is the main site. Molecules that maintain intracellular Ca^{2+} homeostasis include diverse Ca^{2+} channels, pumps, exchangers and binding proteins, collectively known as the Ca^{2+} signaling "toolkit." On the background of normal Ca^{2+} homeostasis, oscillations in cytosolic Ca^{2+} levels that vary in amplitude, frequency and duration translate into specific cellular effects.[1]

The principles of intracellular Ca^{2+} homeostasis in MKs are similar to those in other cells. MK surface receptors activate phospholipase C (PLC) that generates inositol 1,4,5-trisphosphate (IP3).[2,3] IP3 binds to IP3 receptors (IP3Rs) located on the ER membrane, triggering the release of Ca^{2+} from the ER. Depleted ER Ca^{2+} stores are refilled from the extracellular space through the process called store-operated calcium entry (SOCE), facilitated by stromal interaction molecule 1 (STIM1). STIM1 recruits ORAI1 channels in the plasma membrane that refill ER Ca^{2+} stores. High levels of cytosolic Ca^{2+} that arise during cell activation are normalized by two main types of Ca^{2+} pumps that either transport Ca^{2+} back to the extracellular space (plasma membrane Ca^{2+} ATPases [PMCA]) or to the ER (sarco-/endo-plasmic reticulum Ca^{2+} ATPases [SERCA]).[4]

Both ER Ca^{2+} release and SOCE are known to regulate MK development and maturation. In megakaryocytic progenitors, sustained SOCE activates the calcineurin-nuclear factor of activated T cells (NFAT) pathway that inhibits cell proliferation.[5] In mature MKs, SOCE supports MK migration, and ER Ca^{2+} release triggers MK adhesion and proplatelet formation.[6] SOCE represents the main pathway for Ca^{2+} entry in most cells, but MKs also express other Ca^{2+} channels located in the plasma membrane, including transient receptor potential cation (TRPC) and *N*-methyl-D-aspartate (NMDA) receptors (NMDARs), the roles of which are much less understood.

NMDARs are glutamate gated, nonspecific cation channels with high Ca^{2+} permeability.[7] The first evidence that NMDARs operate as ion channels in MKs was obtained by Genever et al, who demonstrated that tritiated MK-801 injected into mice intracardially bound to MKs in the bone marrow examined 15 minutes later.[8] Because MK-801 can only bind within an open NMDAR pore,[9] its labeling of MKs was consistent with the NMDAR function as ion channel in these cells. Later, we showed that glutamate, NMDA and glycine induce Ca^{2+} fluxes in Meg-01 cells, and NMDAR blockers (memantine and MK-801) counteract this effect.[10,11] Others and we also found that memantine and MK-801 inhibit differentiation of normal mouse and human MKs *ex vivo* but induce differentiation of leukemic Meg-01 cells *in vitro*.[8,10–12] Further characterization of NMDAR effects using chemical modulators was restricted by toxic, likely off-target effects. Thus, we undertook a gene knockout approach in Meg-01 cells.

We hypothesized that NMDAR-mediated Ca^{2+} influx contributes to intracellular Ca^{2+} homeostasis in megakaryocytic cells, which impacts the transcriptional program of cell differentiation. Using CRISPR-Cas9, we attenuated NMDAR function in a Meg-01 cell line as a model of megakaryocytic-erythroid progenitors and examined subsequent effects on cell phenotype. Our results suggest an important role of intracellular Ca^{2+} homeostasis in balancing megakaryocytic-erythroid differentiation.

Methods

Cell Culture

Meg-01 cells (German Collection of Microorganisms and Cell Cultures, Braunschweig, Germany) were used as models of human megakaryocytic-erythroid progenitors. Meg-01 cell line is derived from acute megakaryoblastic leukemia transformed from chronic myeloid leukemia, but cells undergo megakaryocytic differentiation.[13–15] Meg-01 and Meg-01-*GRIN1*$^{-/-}$ cells were maintained at 37°C, 5% CO_2, in RPMI-1640 medium supplemented with 2 mM L-glutamine and 10% foetal bovine serum (FBS; all from Thermo Fisher Scientific, Waltham, Massachusetts, United States), as described previously.[10] To induce differentiation, cells were cultured in the presence of phorbol-12-myristate-13-acetate (10 nM; PMA; Sigma–Aldrich, Saint Louis, Missouri, United States) for 72 hours. TrypLE (Thermo Fisher Scientific) was used to collect adherent cells for analysis. Cultures were confirmed to be free from mycoplasma infection using LookOut Mycoplasma PCR Detection Kit (Sigma–Aldrich).

CRISPR-Cas9 Plasmid Design and Transfection

The CRISPR-Cas9 system was applied using a single guide RNA (gRNA) to induce an insertion/deletion (INDEL) causing a frameshift in the *GRIN1* gene. The genomic target sequence was positioned in exon 1 of *GRIN1*, downstream of all known start codons for the gene. The sequence 5′-CAAGATCGTCAACATTGGCG-3′ was cloned into a modified pMIG plasmid containing an orange fluorescent protein (OFP) reporter sequence (pMIG-Alpha was a gift from William Hahn, Addgene plasmid #9044; http://n2t.net/addgene:9044 RRID: Addgene_9044; Addgene, Watertown, Massachusetts, United States).[16] Meg-01 cells were transfected with an endotoxin free preparation of the plasmid using Lipofectamine 3000 (Thermo Fisher Scientific). After 48 hours, single, high OFP expressing cells were sorted into 96-well plates using the FACSAria II (Becton Dickson, Franknlin Lakes, New Jersey, United States). Cells were cultured in RPMI-1640 supplemented with 2 mM Glutamax, 25 mM HEPES (4-[2-hydroxyethyl]-1-piperazineethanesulfonic acid), 1 mM sodium pyruvate and 40% FBS for 2 weeks. The DNA from the clones was amplified using primers (forward: 5′-CTCCGACACACACGCTCAC-3′, reverse: 5′-ATAGGCGAGCCAGCAGACC-3′) targeting the gRNA target site, and amplicons were screened for INDELs by Sanger sequencing.

Transfection of Short Interfering RNA

Meg-01 cells were plated at 6×10^5 cells per well in a six-well plate and allowed to adhere for 4 hours. Endoribonuclease-prepared short interfering RNA (esiRNA) targeting *GRIN1* (esi*GRIN1*; EHU157091, Sigma–Aldrich) were used to transiently knockdown *GRIN1* in Meg-01 cells. Transfections were done in serum-free OptiMEM media assisted by Lipofectamine RNAimax (both from Thermo Fisher Scientific). OptiMEM was replaced with complete culture media 12 hours after transfections, and cells were harvested for analysis 60 hours later.[17]

[^{3}H]MK-801 Binding Assay

[^{3}H]MK-801 was used to label open (i.e. active) NMDARs. Cells were plated at 5×10^5 cells per well in 24-well plates and allowed to adhere for 4 hours. [^{3}H]MK-801 (5 nM, 1 µCi L^{-1}) (Perkin Elmer, Waltham, Massachusetts, United States) and glutamate 500 µM (NMDAR agonist; Sigma–Aldrich) were added and incubated with cells for 1 hour. Media was removed, cells were washed with serum-free media, and solubilized with 1 N NaOH. β-particle emission was recorded as counts per second using a Wallac Microbeta 1450–021 TriLux Luminometer Liquid Scintillation Counter (LabEquip, Markham, Canada) as described previously.[17]

Cell Viability, Proliferation and Cell Death Assays

Cell viability and proliferation assays were done as previously described.[11] Briefly, cells were seeded at 1×10^4 cells per well in 96-well plates and cultured for 72 hours prior to testing using an MTT kit (Thermo Fisher Scientific). Cell proliferation was examined using the Cell Proliferation ELISA BrdU kit (Roche, Basel, Switzerland) after incubation with bromodeoxyuridine (BrdU) for 6 hours. Cytotoxicity was measured using the Cytotoxicity Detection KitPLUS (lactate dehydrogenase [LDH] release assay; Roche). Selected cell survival assays used the following chemicals: NMDA (synthetic NMDAR agonist, 100 µM), L-glutamate (main NMDAR agonist, 500 µM; both from Sigma–Aldrich), glycine (NMDAR co-agonist, 300 µM; VWR International, Radnor, Pennsylvania, United States), memantine (NMDAR antagonist, 100 µM; Sigma–Aldrich), and cytarabine (0.1 µM; Cayman Chemical, Ann Arbor, Michigan, United States).

Recordings of Intracellular Calcium Responses

Intracellular Ca^{2+} responses were monitored using the Fura-2 Calcium Assay Kit (Abcam, Cambridge, United Kingdom). Cells were plated in poly-D-lysine (Sigma–Aldrich) treated glass-bottom, black, 96-well plates at 9×10^4 cells per well. Cells were allowed to adhere for 4 hours, then washed with 1× Hank's Balanced Salt Solution (HBSS), and loaded with Fura-2-AM at 37°C for 1 hour in the dark. Fluorescence was measured using a 510 nm emission filter with 340 and 380 nm excitation filters from the bottom of the plate with a Tecan Spark Multiplate Reader (Tecan, Männedorf, Switzerland) at 37°C, 5% CO_2. Signals were acquired every second for 30 seconds to establish a baseline and then again every second for a further 120 seconds after the addition of NMDA (100 µM) with glycine (300 µM) or glutamate (500 µM) with glycine (300 µM), both with or without BAPTA (5 mM; 1,2-bis(o-aminophenoxy)ethane-N,N,N′,N′-tetraacetic acid, cell-impermeant calcium chelator; Thermo Fisher Scientific). Other experiments used thapsigargin (2 µM) and ionomycin (5 µg mL^{-1}; both from Sigma–Aldrich).

To measure SOCE fluxes, cells were seeded at 2×10^4 cells per well and cultured for 3 days. Cells were washed with 1× physiological saline prior to loading with Fura-2-AM as above. Ca^{2+} signals were measured every 30 seconds for 5 minutes to establish a baseline. Media was then changed to Ca^{2+} and Mg^{2+} free physiological saline, supplemented with cyclopiazonic acid (10 µM; a SERCA inhibitor that depletes ER Ca^{2+} stores) and EGTA (500 µM; ethylene glycol-bis(β-aminoethyl ether)-N,N,N′,N′-tetraacetic acid, a cell-impermeant calcium chelator; both from Sigma–Aldrich), and signals were recorded every 30 seconds for 7.5 minutes. Media was then changed to physiological saline, and monitoring continued every 30 seconds for a further 12.5 minutes. Fluorescence was measured using a 510 nm emission filter with 340 and 380 nm excitation filters as above. Relative intracellular Ca^{2+} levels were determined, based on the measurement of a fluorescent 340/380 nm ratio.

Flow Cytometry

Nuclear ploidy analysis was performed by staining cells (0.5–1×10^5 per tube) with propidium iodide 50 µg mL^{-1} in a hypotonic sodium citrate buffer (0.1%) for 35 minutes on ice. Cells were washed, resuspended in RPMI-1640, and treated with RNAse 50 µg mL^{-1} at room temperature (RT) for 30 minutes.

The following antibodies (catolog number) were used to characterize myeloid antigen expression: CD13 (561698), CD33 (561816), CD41 (555466), CD42a (558819), CD42b (555473), CD61 (555754), CD71 (347513) (all from BD Biosciences, San Jose, California, United States) and CD235a (IM2212; from Beckman Coulter, Bea, California, United States). Cells (0.5–1×10^5) were incubated with the antibodies for 15 minutes at RT, washed with wash buffer (1× phosphate buffered saline [PBS], 2% FBS, 0.02% sodium azide), and fixed with 0.5% paraformaldehyde (PFA) in 1× PBS.

ER-Tracker Red (10 µM) and LysoTracker Red DNA-99 (50 nM) (both from Thermo Fisher Scientific) were incubated with cells (0.5–1×10^5) at 37°C, 5% CO_2 for 45 and 60 minutes, respectively. Cells were washed with wash buffer and fixed with 0.5% PFA in 1× PBS. All flow cytometry data were acquired on the BD LSRII flow cytometer and analyzed using BD FACSDiVa software v6.1.1.

Microscopy Examination and Ultrastructure

For immunofluorescence, cells were fixed in 4% PFA in 1× PBS for 15 to 20 minutes and permeabilized for 5 minutes with 0.1% Triton X-100 in PBS. Cells were blocked for 30 minutes with 5% goat serum and then incubated with primary antibodies (CD63 1:200, ab59479, Abcam; GluN1 1:500, MAB363, Merk & Co, Kenilworth, New Jersey, United States or Calnexin 1:1000, ab22595, Abcam) at 4°C overnight. After washing, cells were incubated with 2.5 µg mL^{-1} Dylight 488/594-conjugated secondary antibodies (ab96931 and ab96885, respectively; both from Abcam) for 3 hours. Giemsa staining was performed

using the Cytopro autostainer (ELITech, Paris, France). Bright-field and immunofluorescence microscopy was conducted using an Eclipse Ni-E microscope (Nikon, Tokyo, Japan). Hoffman and phase contrast images were taken on an Eclipse Ti microscope (Nikon).

Transmission electron microscopy was done as previously described.[18] Briefly, cells were fixed with 0.2% glutaraldehyde and 2% PFA in White's saline. Sections were counterstained with uranyl acetate and examined with a Tecnai G2 Spirit Twin transmission electron microscope (FEI Company, Hillsboro, Oregon, United States).

Western Blotting

Cells were lysed in radio-immunoprecipitation assay buffer (50 mM Tris pH 4.7, 150 mM NaCl, 1% NP-40, 0.25% Na-deoxycholate, and 1 mM EDTA) with protease and phosphatase inhibitors (Sigma–Aldrich). Cell lysates were quantified using the Pierce BCA protein asay kit (Thermo Fisher Scientific), and proteins were resolved on a 4 to 15% SDS-PAGE gradient gel. Separated proteins were electrophoretically transferred onto polyvinylidene difluoride membranes for subsequent probing with antibodies (CD63 1:1000, ab59479, Abcam; LC3-II 1:1000, CTE4108S, Thermo Fisher Scientific; pan-Actin 1:10000, MAB1501, Abcam). Membranes were washed and incubated with horseradish peroxidase conjugated secondary antibodies (111–035–003, Jackson ImmunoResearch, Pennyslvania, United States). Clarity Western ECL (Bio-Rad, Hercules, California, United States) was used for signal detection using Chemidoc Touch (Bio-Rad). Membranes were stained with Coomassie Blue to observe total protein. Relative protein quantitation was performed by band densitometry using ImageLab 5.2.1 (Bio-Rad); LC3-II was quantified relative to actin, and CD63 relative to total protein after Coomassie staining.

RNA Isolation, complementary DNA Synthesis, and Reverse Transcriptase-Polymerase Chain Reaction

Total RNA was isolated from cells using TRIzol and the PureLink RNA Mini Kit (both from Thermo Fisher Scientific) following the manufacturer's instructions. On-column DNase digestion was performed using the Purelink DNase set (Thermo Fisher Scientific). Complementary DNA (cDNA) was synthesized using the Quanta qScript XLT cDNA SuperMix (Quantabio, Beverley, Massachusetts, United States). Reverse Transcriptase-quantitative Polymerase Chain Reaction (RT-qPCR) was performed in 10 µL reactions using SYBR Select Master Mix (Thermo Fisher Scientific) for ER stress expression and Perfecta SYBR Green FastMix (Quantabio) for *GRIN1* expression and microarray validation, run on the QuantStudio 12K Flex Real-Time PCR instrument (Thermo Fisher Scientific). Relative expression levels of each gene were normalized to *LMNA*, *HPRT1* and *GAPDH* housekeeping genes, chosen as they remained invariant in our RNA microarray analysis. Relative changes to unmodified Meg-01 cells were calculated using the $2^{-\Delta\Delta Ct}$ method.[19] At least three biological replicates were included for each condition in each experiment. Primer sequences used for the genes encoding ER stress markers,[20] NMDAR subunits,[18] LMNA,[21] and HPRT1[22] were as previously published. Microarray validation was performed using PrimeTime qPCR primer assays from Integrated DNA Technologies (Coralville, Iowa, United States); all primer details are in ►**Supplementary Table S1** (available in the online version).

Gene Expression Profiling and Gene Ontology Analysis

RNA was isolated as described above. Gene expression profiling was performed using the Clariom S microarray assay (Thermo Fisher Scientific). Data were normalized by gene level Robust Multi-array Average method.[23] Unmodified Meg-01 and Meg-01-*GRIN1*$^{-/-}$ cells were assayed in triplicate. Differentially expressed (DE) genes were identified using eBays one-way analysis of variance (ANOVA) with a Benjamini-Hochberg false discovery rate (FDR) of 0.05; analysis was done using Transcriptome Analysis Console 4.0 (Thermo Fisher Scientific).

The overrepresentation enrichment analysis was performed on DE genes with a high fold change ($\geq$2.0) to identify whether any gene ontology (GO) defined biological processes occurred more than chance would dictate. The GO–Slim set-up was selected to reduce the overlap between the GO processes. The over-representation analysis was performed using the PANTHER V14.1 online tool (http://pantherdb.org; accessed May 2019). A more relaxed cutoff (fold change $\geq$ 1.5; FDR $\leq$ 0.05) was applied to interrogate expression of genes within the deregulated biological processes, in particular genes coding for the Ca^{2+} toolkit and hematopoietic transcription factors. Statistical enrichment was determined via Fischer's exact test; a conservative Bonferroni correction was applied to all nominal *p*-values.

Statistical Analysis

Data are expressed as mean $\pm$ standard error of the mean (SEM). Statistical analyses were conducted using GraphPad Prism 8.0 (San Diego, California, United States). Differences in group means were compared with either a Student's *t*-test (two-tailed) or one-way ANOVA with Dunnett *post hoc* for continuous variables, as indicated in figure legends. An α of 0.05 was considered statistically significant.

Results

Generating a Model of Reduced NMDAR Expression in Megakaryocytic Cells

Using CRISPR-Cas9, we knocked out the expression of the *GRIN1* gene in Meg-01 cells; *GRIN1* encodes an obligate, GluN1 subunit of the NMDAR. A pMIG plasmid was modified to carry gRNA targeting exon 1 of *GRIN1*. Forty-eight hours after transfection, Meg-01 cells showing high expression of the OFP reporter were sorted by flow cytometry and grown into single cell colonies. Candidate cell clones were screened by Sanger sequencing of the modified genetic region. A clone was identified with a 59 bp deletion in both *GRIN1* alleles, predicted to cause a frame-shift and premature stop codons in exons 2 and 3 of *GRIN1* (Meg-01-*GRIN1*$^{-/-}$ cells; ►**Fig. 1A**).

Examination by RT-qPCR demonstrated a 91 $\pm$ 3% knockdown of *GRIN1* mRNA compared with unmodified Meg-01 cells (►**Fig. 1Bi**). Binding of [^{3}H]MK-801, use-dependent NMDAR antagonist, was reduced by 72 $\pm$ 16%, indicating low numbers of remaining functional NMDARs (►**Fig. 1Bii**).

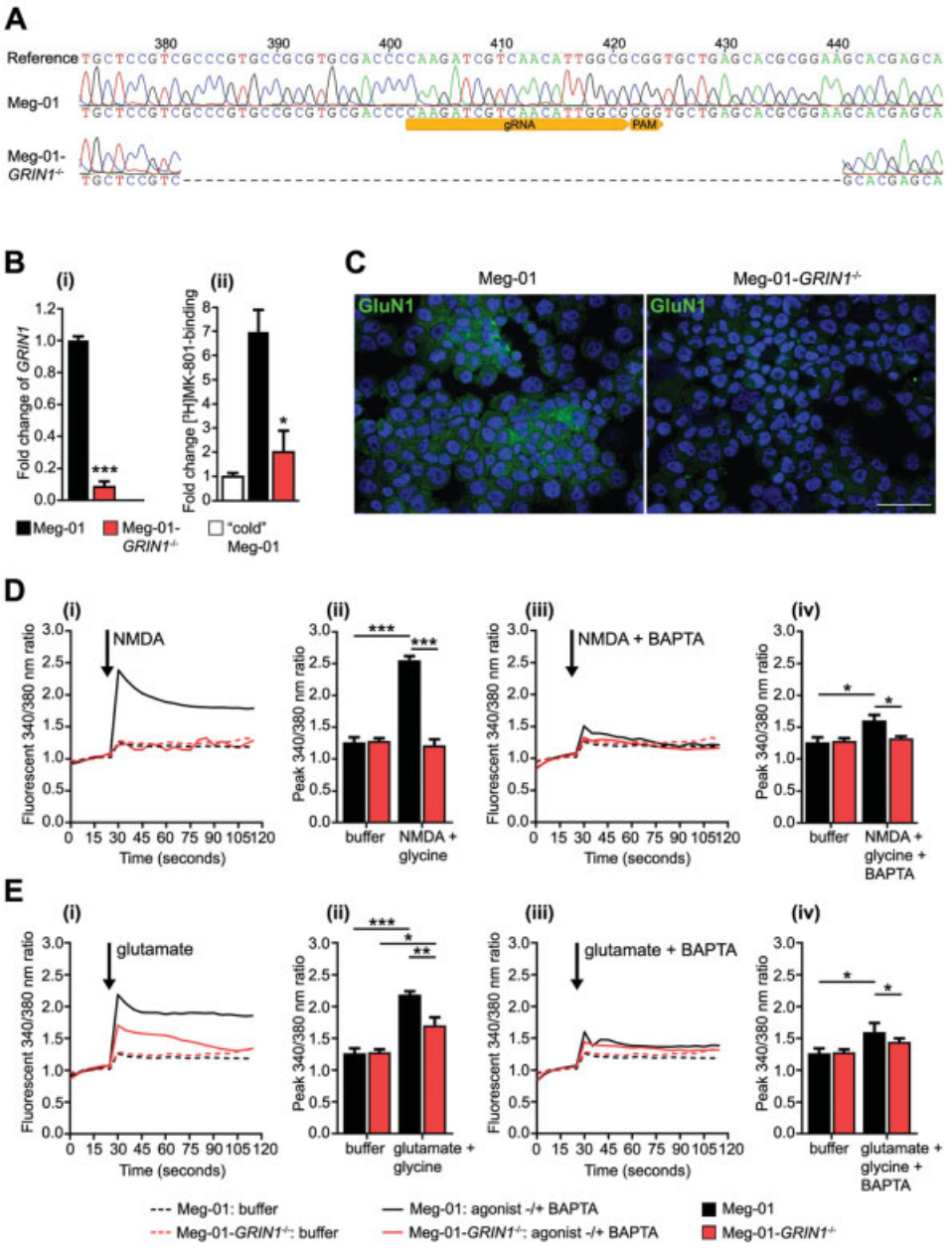

Fig. 1 Validation of the *GRIN1* knockout in Meg-01 cells (Meg-01-*GRIN1*$^{-/-}$ cells). (**A**) Sequence alignment of Sanger sequences obtained from unmodified Meg-01 cells and Meg-01-*GRIN1*$^{-/-}$ cells to the *GRIN1* reference sequence (National Center for Biotechnology Information accession number NG_011507.1) for nucleotides 373–449 (exon 1). The dashed line indicates the region of gene deletion (59 bp) generated by CRISPR-Cas9. The relative positions of the guide RNA (gRNA) target and protospacer adjacent motif (PAM) sequences are shown (yellow arrows). (**B**) Bar graphs showing relative levels of *GRIN1* mRNA expression examined by RT-qPCR (**i**) and [^{3}H]MK-801 binding (**ii**) in Meg-01-*GRIN1*$^{-/-}$ cells, calculated relative to unmodified Meg-01 cells. Bars are mean ± standard error of the mean from four independent experiments for RT-qPCR and two for [^{3}H]MK-801 binding, each in triplicate. "Cold" Meg-01 indicates [^{3}H]MK-801 binding by Meg-01 cells after incubation with nonradioactive ("cold") MK-801 (specificity control). (**C**) Representative images showing GluN1 immunofluorescence staining in Meg-01 and Meg-01-*GRIN1*$^{-/-}$ cells. Scale bar, 50 µM for both. (**D, E**) NMDAR-mediated intracellular calcium responses were measured relative to baseline set at (1.0) in Meg-01 and Meg-01-*GRIN1*$^{-/-}$ cells. Cells were loaded with Fura-2-AM and stimulated with NMDAR agonists in the presence of extracellular Ca^{2+}: NMDA 100 µM without and with BAPTA 10 mM **D** (**i**, **ii**, **iii** and **iv**, respectively); and glutamate 500 µM without and with BAPTA 10 mM **E** (**i**, **ii**, **iii** and **iv**, respectively). Line graphs in D and E show the mean fluorescent 340/380 nm ratio of Fura-2 recorded over 120 seconds corresponding bar graphs show the peak level (mean ± standard error of the mean) of the fluorescent 340/380 nm ratio recorded during the observation period. Buffer indicates control. Each experimental condition was repeated five times, in triplicate. Statistical significance is shown (Student's *t*-test for B and one-way ANOVA with Dunnett *post hoc* for D and E; $^{*}p < 0.05$, $^{**}p < 0.01$, $^{***}p < 0.001$). BAPTA, 1,2-bis(o-aminophenoxy) ethane-N,N,N,N-tetraacetic acid; gRNA, guide RNA; NMDAR, *N*-methyl-D-aspartate receptor; PAM, protospacer adjacent motif; RT-qPCR, quantitative reverse transcriptase-polymerase chain reaction.

Immunofluorescence demonstrated minimal staining for the GluN1 protein (►**Fig. 1C**). The virtual loss of Ca^{2+} influx through NMDAR was confirmed by the examination of Ca^{2+} fluxes in Fura-2-AM loaded cells (►**Fig. 1D** and **E**). No Ca^{2+} influx was recorded in Meg-01-*GRIN1*$^{-/-}$ cells in response to 100 µM NMDA (synthetic but specific NMDAR agonist; ►**Fig. 1Di–ii**). Peak Ca^{2+} responses to 500 µM glutamate (endogenous but nonspecific NMDAR agonist) were 54% lower in Meg-01-*GRIN1*$^{-/-}$ cells compared with unmodified Meg-01 cells (►**Fig. 1Ei–ii**), implying contribution from other glutamate receptors. The effect of *GRIN1* deletion on NMDAR-evoked Ca^{2+} influx resembled that of memantine (NMDAR blocker), supporting that Meg-01-*GRIN1*$^{-/-}$ cells provided a valid model of reduced NMDAR-mediated Ca^{2+}entry in Meg-01 cells (►**Supplementary Fig. S1**, available in the online version).

Loss of *N*-Methyl-D-Aspartate Receptor Function Has an Antiproliferative and Proapoptotic Effect

Morphologically, Meg-01-*GRIN1*$^{-/-}$ cells were larger, more adherent, and multiplied visibly slower, compared with unmodified Meg-01 cells (►**Fig. 2A**; ►**Videos 1** and **2**). Congruently, MTT activity and BrdU incorporation were lower, confirming reduced cell numbers and proliferation respectively (►**Fig. 2B** and **C**). When culture media was supplemented with NMDA (100 µM) or glutamate (500 µM), proliferation of unmodified Meg-01 cells increased but not of Meg-01-*GRIN1*$^{-/-}$ cells (►**Fig. 2C**), providing additional evidence that the *GRIN1* knockout reduced NMDAR function. LDH release was higher for Meg-01-*GRIN1*$^{-/-}$ cells during normal culture, implying an increased level of basal cell death (►**Fig. 2D**).

Video 1

Growth pattern of Meg-01 cells in culture over 24-hour period. Time-lapse microscopy was performed using a Nikon TE2000E inverted microscope equipped with an automated stage, a 20X 0.25 numerical aperture Hoffman modulation contrast objective, and a Solent incubation system (37°C, 5% CO2; Solent Scientific Limited, Portsmouth, United Kingdom). Cells were grown in RPMI-1640 supplemented with 10% FBS. Images were acquired every 10 minutes over 24 hours and videos were assembled using NIS-Elements (Nikon). Online content including video sequences viewable at: https://www.thieme-connect.com/products/ejournals/html/10.1055/s-0040-1708483.

Video 2

Growth pattern of Meg-01-*GRIN1*$^{-/-}$ cells in culture over 24-hour period. Time-lapse microscopy was performed as for ►**Video 1**. Online content including video sequences viewable at: https://www.thieme-connect.com/products/ejournals/html/10.1055/s-0040-1708483.

Flow cytometric measurement of DNA content after staining with propidium iodide showed increased ploidy in Meg-01-*GRIN1*$^{-/-}$ cells, suggesting megakaryocytic differentiation (►**Fig. 2E**). However, unexpectedly, expression of megakaryocytic markers (CD41a, CD61; ►**Fig. 2F** and **Gi–ii**; ►**Supplementary Fig. S2**, available in the online version) and CD42a and CD42b (►**Supplementary Figs S3** and **S4**, available in the online version) were lower. Instead, erythroid markers (CD235a and CD71) were higher, implying increased differentiation toward the erythroid lineage (►**Fig. 2F** and **Giii–iv**; ►**Supplementary Figs S5** and **S6**, available in the online version).

Other distinctive features of Meg-01-*GRIN1*$^{-/-}$ cells included progressive accumulation of cytoplasmic vacuoles and granules (►**Fig. 3**). Some vacuoles were small, located mostly in the perinuclear location (►**Fig. 3A** and **B**; black arrowheads), others were large, distributed throughout the cytoplasm (►**Fig. 3A** and **B**; black arrows). Transmission electron microscopy was performed to clarify the cytoplasmic content, which revealed that some cells were filled with vacuolar-like structures, including frequent immature dense granules (►**Fig. 3C**; blue arrowheads). Staining with CD63 and LysoTracker was increased, confirming accumulation of lysosome-related organelles (►**Fig. 4A–C**; ►**Supplementary Fig. S7A** and **B**, available in the online version); in Meg-01 cells these are known to include both lysosomes and developing dense granules.[24] The lysosomal accumulation raised the possibility of increased autophagy, the induction of which was confirmed by higher lipidation of microtubule associated protein 1 light chain 3 (LC3) compared with unmodified Meg-01 cells (►**Fig. 4D**; ►**Supplementary Fig. S8**, available in the online version). The ER-Tracker staining was increased in Meg-01-*GRIN1*$^{-/-}$ cells when tested by flow cytometry suggesting ER expansion (►**Fig. 4E**; ►**Supplementary Fig. S7C**, available in the online version), corroborated by Calnexin immunofluorescence (►**Supplementary Fig. S9**, available in the online version). The ER expansion suggested ER stress, which was confirmed by RT-qPCR of selected ER stress markers (►**Fig. 4F**). In contrast to the increased presence of dense granules in Meg-01-*GRIN1*$^{-/-}$ cells, there was no evidence that α-granules accumulated, as expression of P-selectin (CD62P) and von Willebrand factor remained low (►**Supplementary Fig. S10**, available in the online version).

Intracellular Calcium Homeostasis is Disturbed in Meg-01-*GRIN1*$^{-/-}$ Cells

Intracellular Ca^{2+} transients were measured in cells loaded with Fura 2-AM (►**Fig. 5**). We found that compared with unmodified Meg-01 cells, Meg-01-*GRIN1*$^{-/-}$ cells had elevated cytosolic Ca^{2+} levels at baseline (►**Fig. 5Ai** and **Aii**). In contrast, an effect of ER Ca^{2+} release tested in the presence of cyclopiazonic acid (an inhibitor of SERCA) was reduced (►**Fig. 5Ai** and **Aiii**). Similarly, the SOCE effect, measured after re-addition of extracellular Ca^{2+}, was lower (►**Fig. 5Ai** and **Aiv**). Application of thapsigargin (another SERCA inhibitor) and ionomycin (Ca^{2+} ionophore) confirmed reduced contribution of ER Ca^{2+} in Meg-01-*GRIN1*$^{-/-}$ cells (►**Fig. 5B** and **C**, respectively).

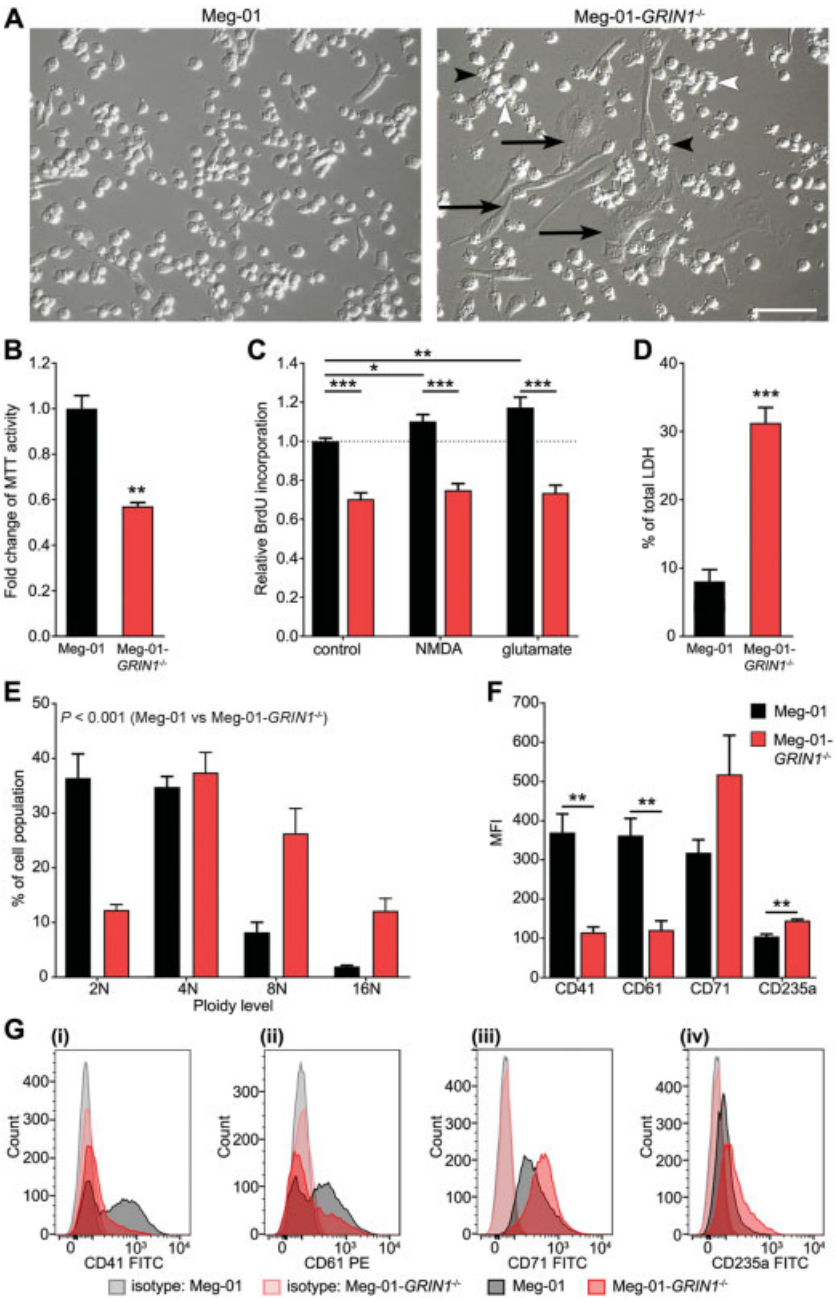

Fig. 2 Effects of *GRIN1* deletion on proliferation and differentiation of Meg-01 cells. (**A**) Representative images of Meg-01 and Meg-01-*GRIN1*$^{-/-}$ cells taken by Hoffman modulation contrast microscopy. Unmodified Meg-01 cells grew mostly singly in suspension. In comparison, Meg-01-*GRIN1*$^{-/-}$ cells were larger, more granular and more adherent. Examples of the following features are pointed to in Meg-01-*GRIN1*$^{-/-}$ cells: cell surface budding (black arrowheads); cell clumping (white arrowheads); large, adherent cells, some with cytoplasmic projections (black arrows). Scale bar, 100 µm for both. (**B–D**) Bar graphs showing numbers of viable cells measured by MTT assay (fold change; B), cell proliferation measured by BrdU assay (relative to control; C) and the percentage cell death measured by the cytotoxicity detection (lactate dehydrogenase; LDH) kit (D) in Meg-01 and Meg-01-*GRIN1*$^{-/-}$ cells cultured for 3 days. In (C), the effect of NMDAR agonists, NMDA 100 µM and glutamate 500 µM, on cell proliferation is also shown. (**E**) Nuclear ploidy level (%) in Meg-01-*GRIN1*$^{-/-}$ and unmodified Meg-01 cells examined by flow cytometry; 2N, 4N, 8N and 16N indicate ploidy classes. (**F, G**) Expression of megakaryocytic and erythroid differentiation markers (CD41a, CD61, CD71 and CD235a) on Meg-01 and Meg-01-*GRIN1*$^{-/-}$ examined by flow cytometry; gating is shown in ►**Supplementary Figs S2**, **S5** and **S6**. G (**i–iv**) Representative histogram examples of differentiation markers shown in (**F**), including isotype controls. All bar graphs show mean ± standard error of the mean from at least three independent experiments. Statistical significance is shown (one-way ANOVA with Dunnett *post hoc*; $^{*}p < 0.05$, $^{**}p < 0.01$, $^{***}p < 0.001$). BrdU, 5-bromo-2-deoxyuridine; MFI, median fluorescent intensity; MTT, 3-(4,5-dimethylthiazol-2-yl)-2,5-diphenyltetrazolium bromide; NMDAR, *N*-methyl-D-aspartate receptor.

Considering that little is known about NMDARs in megakaryocytic cells, we profiled transcriptomic effects of *GRIN1* deletion using Clariom S microarrays (►**Fig. 6**). DE genes were first determined as probe-sets that showed at least a twofold change compared with unmodified Meg-01 cells, with an FDR adjusted p-value ≤ 0.05. The GO analysis identified 248 genes that were upregulated and 187 genes that were downregulated, with four differentially regulated biological processes, of which "Regulation of developmental process" (GO:0050793) and "Cellular calcium ion homeostasis" (GO:0006874) were the

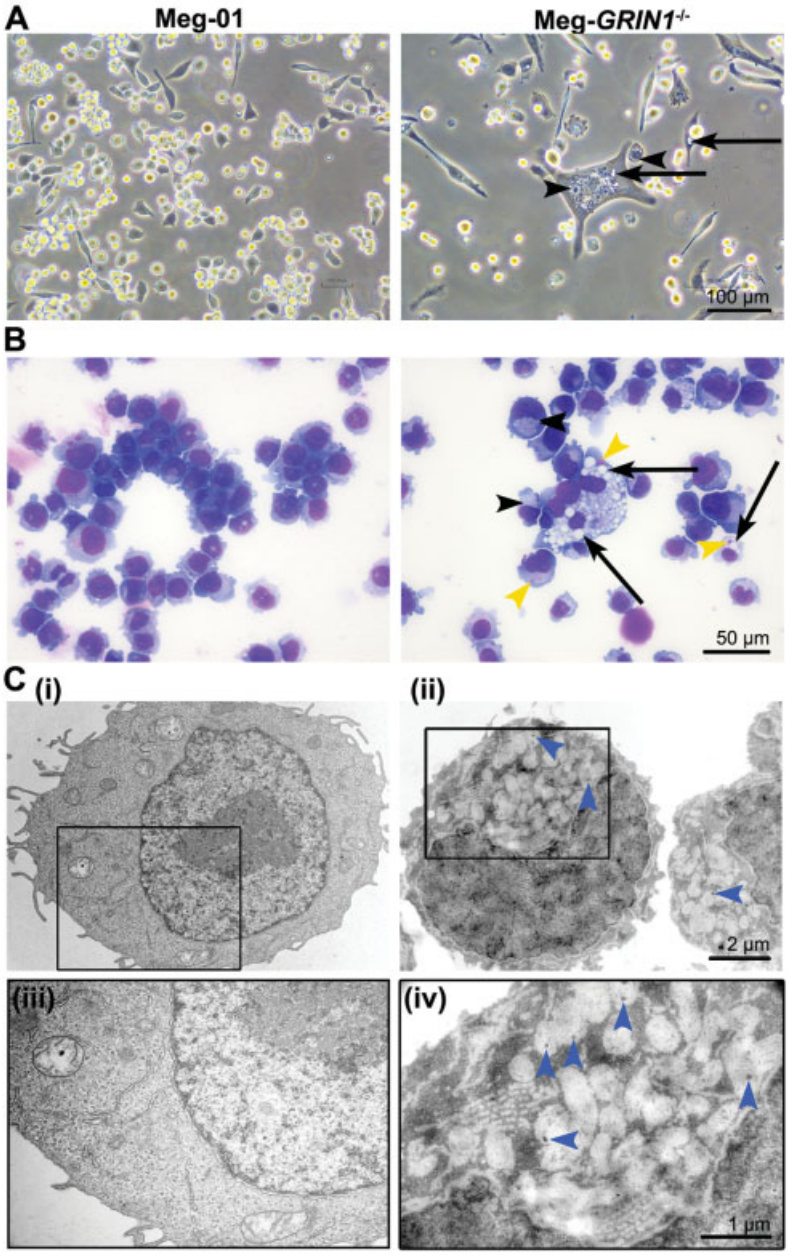

Fig. 3 Cytological effects of *GRIN1* knockout in Meg-01 cells. Representative images of cellular morphology of Meg-01 and Meg-01-*GRIN1*$^{-/-}$ cells visualized by phase contrast microscopy (**A**), bright field microscopy after Wright–Giemsa staining (**B**), and transmission electron microscopy (**C**). Examples of the following morphological features are pointed to in Meg-01-*GRIN1*$^{-/-}$ cells: small, perinuclear cytoplasmic vacuoles (black arrowheads); larger cytoplasmic vacuoles (black arrows); atypical cytoplasmic granules (yellow arrowheads); immature dense granules (blue arrowheads). Frames in **i** and **ii** mark regions enlarged in **iii** and **iv**, respectively. Scale bars are shown.

most deregulated (►**Fig. 6A**; **Supplementary Microarray Excel Data File**, available in the online version). Then we analyzed expression of 82 core transcripts of the Ca^{2+} toolkit, using a list of genes studied in cancer cells before.[25] ►**Supplementary Table S2** (available in the online version) provides data on the expression of all Ca^{2+} toolkit genes we analyzed; here, we summarize the most prominent changes (►**Table 1**).

Meg-01-*GRIN1*$^{-/-}$ cells showed reduced expression of *TRPC6* and *CACNA1A* (coding for TRPC6 and Cav2.1, respectively), while *MCOLN3* (coding for TRP mucolipin 3, TRPML3) was increased (►**Table 1**). TRPC6 contributes to SOCE in MKs.[26] The role of Cav2.1 in MKs is unclear, but in erythrocytes Cav2.1 is regulated by TRPC6 and NMDAR.[27] We also found reduced expression of two genes encoding Ca^{2+} pumps, *ATP2B4* (coding for PMCA4) and *ATP2A3* (coding for SERCA3), as well as *SLC24A3* (coding for K^+-dependent Na^+/ Ca^{2+} exchanger 3, NCKX3; ►**Table 1**). The notable changes affecting Ca^{2+} binding proteins included downregulation of *CALN1* (encoding the ER protein, calneuron 1) and upregulation of *CALB1* and *SCIN* (encoding cytosolic calbindin 1 and scinderin, respectively; ►**Table 1**).

Selected microarray data were validated using RT-qPCR in independent passages of Meg-01-*GRIN1*$^{-/-}$ cells (►**Fig. 6B**,

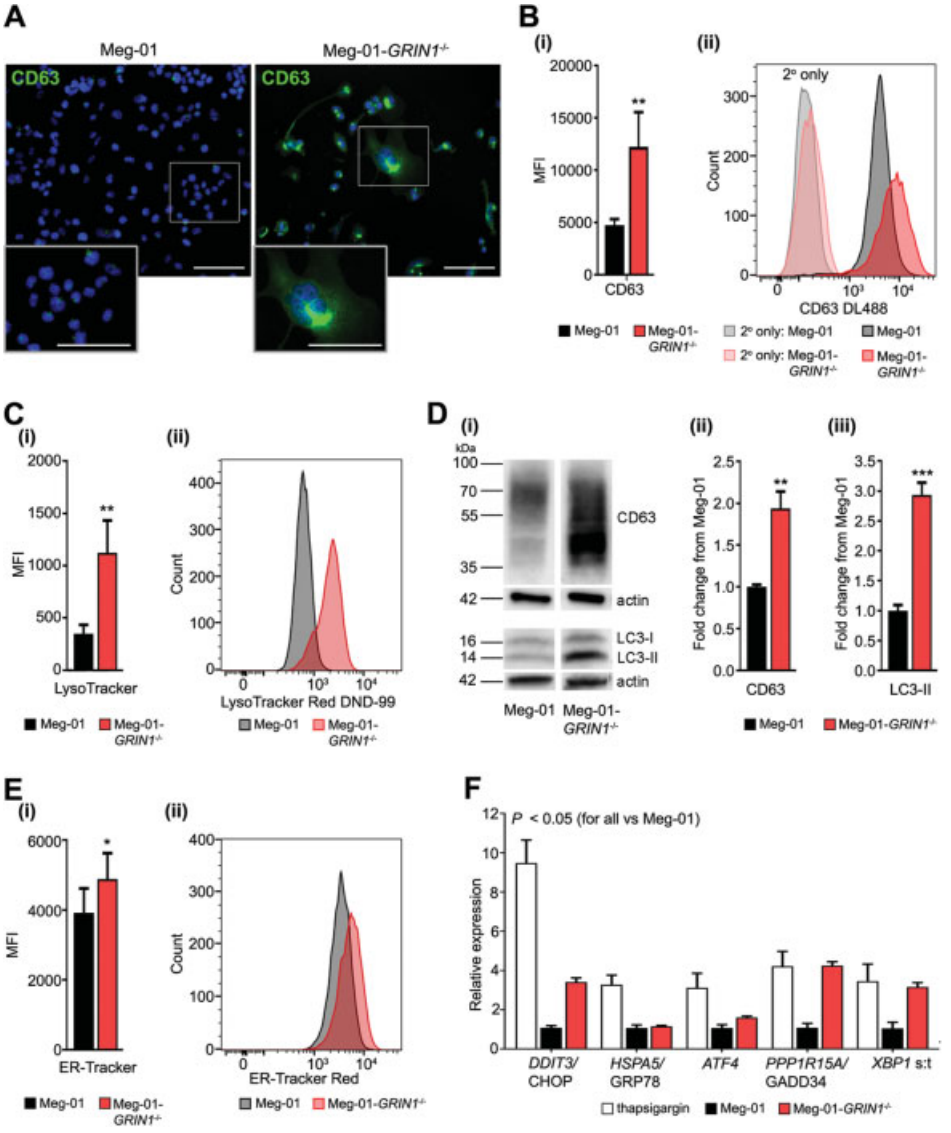

Fig. 4 Cellular stress response pathways examined in Meg-01-*GRIN1*$^{-/-}$ cells. (**A**) Representative images of CD63 immunofluorescence staining in Meg-01 and Meg-01-*GRIN1*$^{-/-}$ cells visualized by fluorescence microscopy. Scale bars, 100 µm. (**B–E**) Bar graphs showing the median fluorescent intensity of CD63 (**Bi**), LysoTracker Red DND-99 (**Ci**), and ER-Tracker Red (**Ei**) in Meg-01 and Meg-01-*GRIN1*$^{-/-}$ cells examined by flow cytometry. Corresponding histograms of representative examples are shown for CD63 expression including secondary antibody only controls (**Bii**) and the level of staining for LysoTracker Red DND-99 (**Cii**) and ER-Tracker Red (**Eii**). At least three independent experiments were performed for each; gating is shown in ►**Supplementary Fig S7**. (**D**) Evidence for autophagy induction in Meg-01-*GRIN1*$^{-/-}$ cells. Expression of CD63 and lipidation of LC3 in Meg-01 and Meg-01-*GRIN1*$^{-/-}$ cells examined by Western blotting (**Di**). Relative expression of CD63 (normalized to total protein; **Dii**) and LC3 lipidation (normalized to β-actin; **Diii**) was determined by band densitometry in Meg-01-*GRIN1*$^{-/-}$ cells, relative to Meg-01 cells. Full blots are shown in ►**Supplementary Fig. S8**. Experiments were performed three times in duplicate. (**F**) Bar graphs showing relative endoplasmic reticulum stress response transcripts examined by RT-qPCR in Meg-01-*GRIN1*$^{-/-}$ cells, calculated relative to unmodified Meg-01 cells. Labels include traditional protein names where relevant. Thapsigargin 2 µM was used as a positive control. XBP1s:t is the ratio of spliced to total XBP1 transcripts. Four independent experiments were performed in triplicate. All bar graphs show mean ± standard error of the mean. Statistical significance is shown (Student's *t*-test; $^{*}p < 0.05$, $^{**}p < 0.01$, $^{**}p < 0.001$). NMDAR, *N*-methyl-D-aspartate receptor; RT-qPCR, quantitative reverse transcriptase-polymerase chain reaction.

pink bars), and in unmodified Meg-01 cells after transient knockdown of *GRIN1* using esi*GRIN1* (►**Fig. 6B**, white bars), or pharmacologic NMDAR inhibition using memantine (►**Supplementary Fig. S11**, available in the online version). Both esi*GRIN1* and memantine recreated the pattern of changes seen in Meg-01-*GRIN1*$^{-/-}$ cells, although esi*GRIN1* effects were weaker (►**Fig. 6B**, white bars), and memantine did not change *CALN1* expression (►**Supplementary Fig. S11**, available in the online version). The effects of memantine argued that altered expression of Ca^{2+} channels and pumps detected in Meg-01-*GRIN1*$^{-/-}$ cells developed due to reduced Ca^{2+} influx; however, lower expression of *CALN1* may have been secondary to a longer term deregulation in intracellular Ca^{2+} handling induced by *GRIN1* deletion. Collectively, our data highlight significant disturbance in the Ca^{2+} regulatory genes in Meg-01-*GRIN1*$^{-/-}$ cells, which underscores the important role of NMDAR in Ca^{2+} homeostasis in the parent cell line.

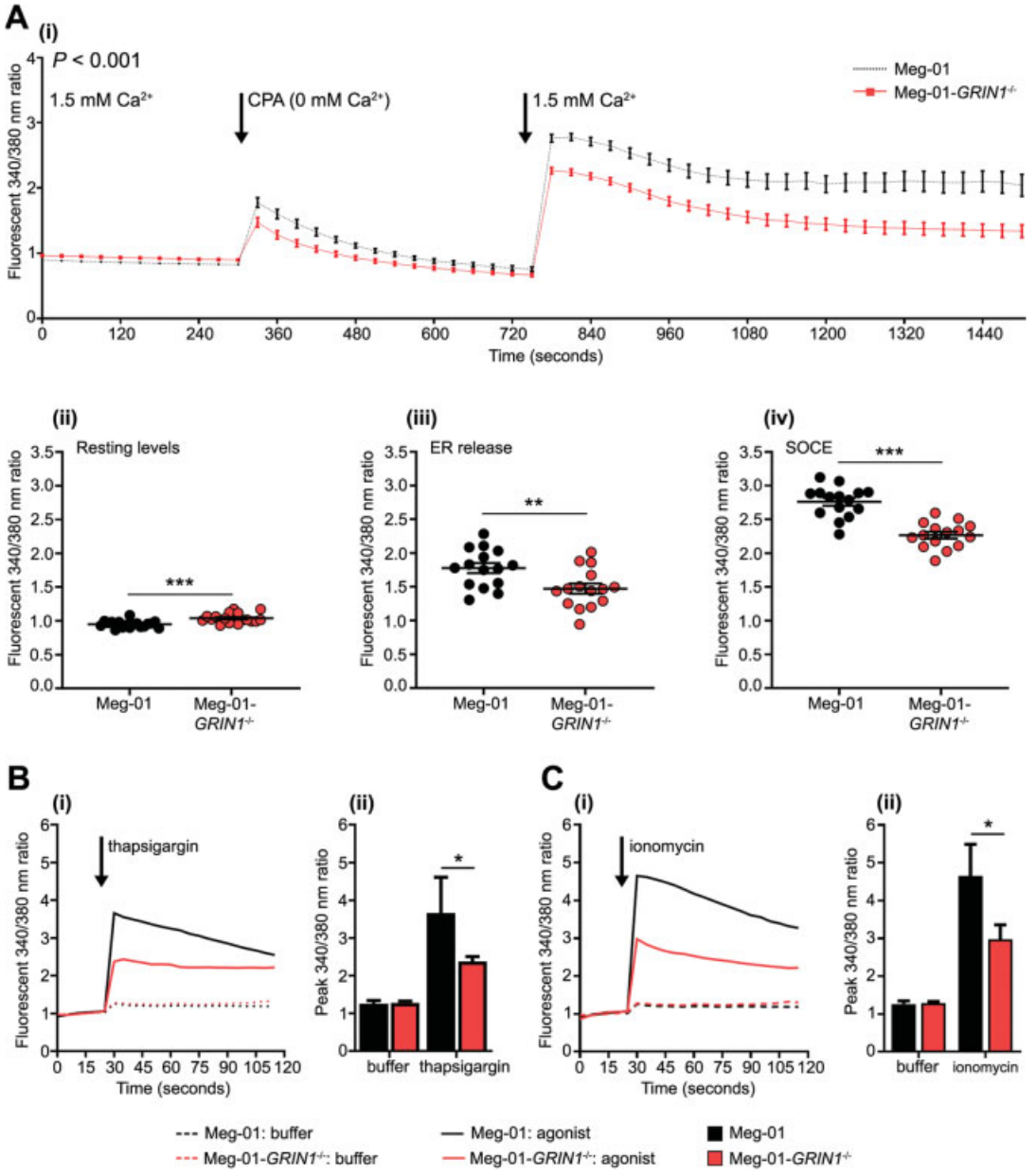

Fig. 5 Effects of *GRIN1* deletion on intracellular calcium responses in Meg-01 cells. (**A–C**) Unmodified Meg-01 and Meg-01-*GRIN1*$^{-/-}$ cells were loaded with Fura-2-AM; relative intracellular Ca^{2+} levels were measured from a fluorescent 340/380 nm ratio. **A** (**i**) Line graph shows mean ± standard error of the mean of the fluorescent 340/380 nm ratio over 1,500 seconds from five independent experiments performed in triplicate. The first 300 seconds reflects relative level of resting cytoplasmic Ca^{2+} (measured in buffer with 1.5 mM Ca^{2+}). At 300 seconds, new buffer was added (containing 0 mM Ca^{2+}, 500 nM EGTA, and 10 µM CPA) to measure an effect of ER store release; at 750 seconds 1.5 mM Ca^{2+} was readded and the store-operated Ca^{2+} entry effect was measured. Dotplots generated from Ai show all individual data points for: resting Ca^{2+} measurements (first 300 seconds [**Aii**]); CPA-induced maximum responses (at 330 seconds [**Aiii**]); and peak responses measured after readdition of extracellular Ca^{2+} (at 780 seconds [**Aiv**]). In separate experiments, Fura-2-AM loaded cells were stimulated with thapsigargin 2 µM (**B**) or ionomycin 5 µg mL^{-1} (**C**) in the absence of extracellular Ca^{2+} to measure an effect of ER Ca^{2+} store release. Buffer indicates control. Line graphs show the mean level of a fluorescent 340/380 nm ratio over 120 seconds. Corresponding bar graphs show the peak level of a fluorescent 340/380 nm ratio during the observation period (mean ± standard error of the mean). Each experimental condition was repeated five times in triplicate. Statistical significance is shown (Student's *t*-test; $^{*}p < 0.05$, $^{**}p < 0.01$, $^{***}p < 0.001$). CPA, cyclopiazonic acid; EGTA, ethylene glycol tetraacetic acid; ER, endoplasmic reticulum.

Transcriptomic Features of Increased Erythroid Differentiation in Meg-01-*GRIN1*$^{-/-}$ Cells

Transcriptome analysis provided further valuable insights into the state of differentiation in Meg-01-*GRIN1*$^{-/-}$ cells. The highest expressed transcription factors were *HEY1*, *ZEB1* and *JUN* (►**Table 2**). Transcripts of Krueppel-like factors, including *KLF1*, a master regulator of erythropoiesis were also increased (►**Table 2**). In contrast, transcription factors favoring megakaryopoiesis (in particular *RUNX1*, *FLI1*, *ERG* and *MEIS1*) were reduced (►**Table 2**). This pattern aligns with reduced megakaryocytic and increased erythroid differentiation we observed in Meg-01-*GRIN1*$^{-/-}$ cells. In keeping with the levels of transcriptional regulators, transcripts of molecules associated with megakaryocytic differentiation (e.g. platelet-associated glycoproteins) were lower, but erythroid transcripts (e.g. embryonic haemoglobins and red cell

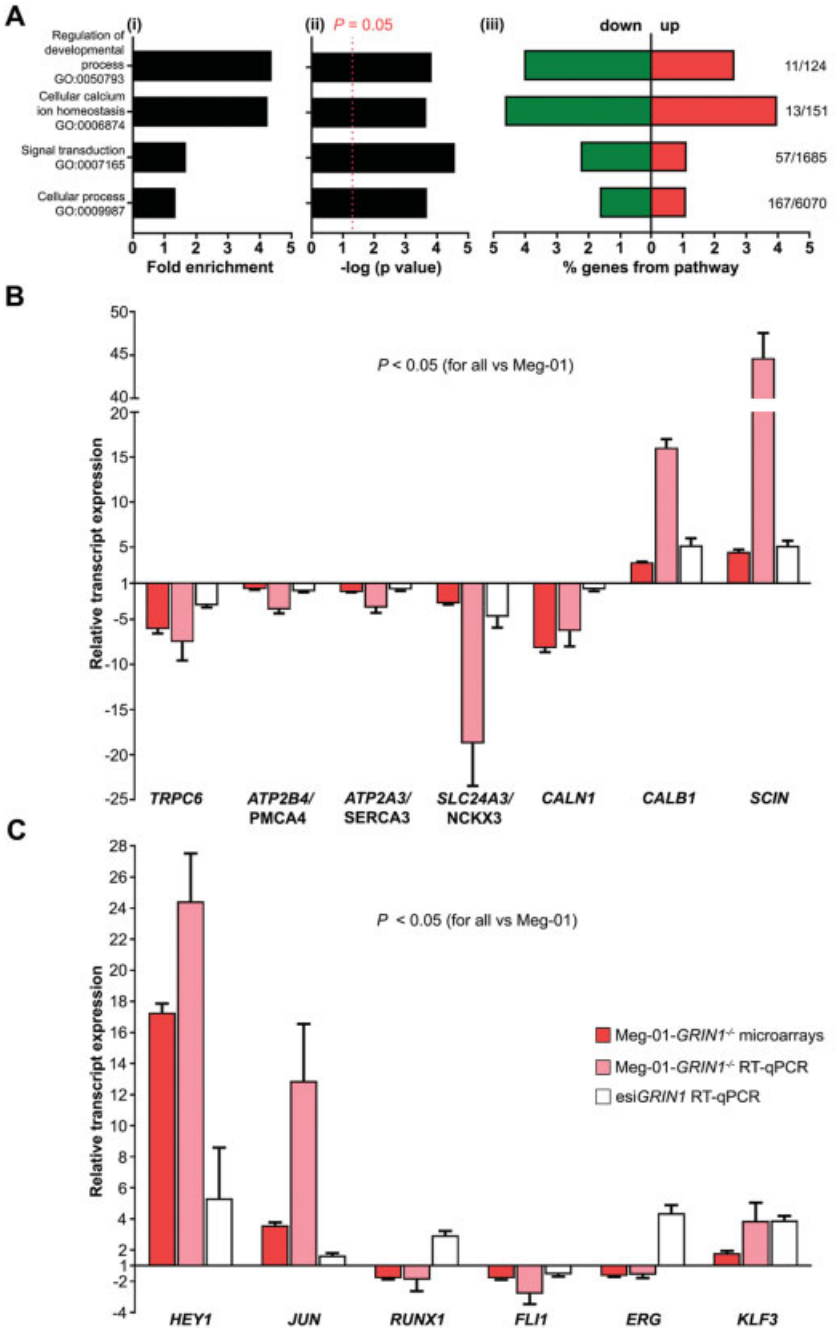

Fig. 6 Transcriptomic changes in Meg-01-*GRIN1*$^{-/-}$ cells determined from Clariom S microarrays. (**A**) Biological processes altered in Meg-01-*GRIN1*$^{-/-}$ cells are shown, identified by GO enrichment analysis performed with the PANTHER tool, using the PANTHER GO-Slim biological process annotation dataset with FDR $\leq$0.05 and fold change $\geq$2. (Ai) Fold enrichment of GO term from reference. (**ii**) Statistical significance of GO term shown as –log (*p*-value). (**iii**) Percentage of genes in the list that were differentially expressed. Numbers on the far right indicate genes differentially expressed over all genes in the pathway. (**B, C**) Bar graphs showing relative transcript levels of selected genes involved in the Ca^{2+} toolkit (B) and deregulated transcription factors (C) detected by microarrays using FDR $\leq$ 0.05 and fold change change $\geq$1.5 (red bars), followed by validation by RT-qPCR in independent biological samples (pink bars), and after treatment with esi*GRIN1* (white bars), all calculated relative to unmodified Meg-01 cells. Positive values indicate increased, and negative values reduced gene expression levels in Meg-01-*GRIN1*$^{-/-}$ cells compared with unmodified Meg-01 cells. In transient knockdown experiments, Meg-01 cells were cultured in the presence of esi*GRIN1* for 3 days. Experiments were repeated three times. Bars are mean $\pm$ standard error of the mean. Labels include traditional protein names where relevant. Statistical significance is shown; Fisher's exact test with FDR correction for (A) and one-way ANOVA with Dunnett *posthoc* for (B) and (C). All differences in expression shown in (B) and (C) were statistically significant compared with unmodified Meg-01 cells. FDR, false discovery rate; GO, gene ontology; RT-qPCR, quantitative reverse transcriptase-polymerase chain reaction; esi*GRIN1,* Meg-01 cells treated with esi (endoribonuclease-prepared short interfering) RNA targeting *GRIN1* gene.

membrane proteins) were higher in Meg-01-*GRIN1*$^{-/-}$ cells compared with unmodified Meg-01 cells (►**Supplementary Table S3**, available in the online version).

Selected changes in transcription factors were confirmed using RT-qPCR (►**Fig. 6C**, pink bars). Effects of esi*GRIN1* were also tested (►**Fig. 6C**, white bars), which showed that

Table 1 Differential expression of the Ca^{2+} toolkit molecules in Meg-01-*GRIN1*$^{-/-}$ cells compared with unmodified Meg-01 cells determined from Clariom S microarrays

Gene name	Calcium toolkit molecule	Fold change	*p*-Value	FDR
SCIN	Scinderin	4.85	1.64E-07	2.41E-05
CALB1	Calbindin 1	3.73	5.26E-08	1.05E-05
MCOLN3	Transient receptor potential mucolipin 3 channel	2.64	0.0003	0.0056
ATP2B4	Plasma membrane Ca^{2+} ATPase 4	−1.78	0.0004	0.0066
ATP2A3	Sarco-/endoplasmic reticulum Ca^{2+} ATPase 3	−1.99	1.04E-07	1.71E-05
CACNA1A	Voltage-gated calcium channel 2.1	−2.26	0.0007	0.0107
SLC24A3	K^+-dependent Na^+/Ca^{2+} exchanger 3	−2.97	1.42E-08	4.29E-06
TRPC6	Transient receptor potential channel 6	−6.61	9.69E-10	6.31E-07
CALN1	Calneuron 1	−8.38	1.24E-10	1.84E-07

Abbreviation: FDR, false discovery rate.

similar to Meg-01-*GRIN1*$^{-/-}$ cells, transcript levels of *HEY1* and *KLF3* were increased 3 days after transfections, and *FLI1* transcripts were reduced. However, *RUNX1* and *ERG* levels were higher, and *JUN* levels increased only slightly upon esi*GRIN1* treatment, suggesting that changes in Meg-01-*GRIN1*$^{-/-}$ cells were time dependent (►**Fig. 6C**). The small upregulation of *JUN* in short-term experiments with esi-*GRIN1* appeared consistent with the known, secondary role of *JUN* after ER stress that we saw in Meg-01-*GRIN1*$^{-/-}$ cells.[28]

The dominant expression of the erythroid transcription factor, *KLF3* persisted in Meg-01-*GRIN1*$^{-/-}$ cells after culture with PMA (►**Supplementary Fig. S12A**, available in the online version). Megakaryocytic differentiation also increased, as it is known to occur in unmodified Meg-01 cells in the presence of PMA (►**Supplementary Figs S12B**, **S13** and **S14**, available in the online version).[14,29] PMA did not affect expression of *TRPC6*, *SLC24A3* and *CALN1* in Meg-01-*GRIN1*$^{-/-}$ cells; however, additional alterations occurred in *ATP2B4*, *ATP2A3* and *CALB1*, which largely followed the direction of change induced by PMA in unmodified Meg-01 cells (►**Supplementary Fig. S12C**, available in the online version). PKC is known to impact Ca^{2+} signaling and interact with Ca^{2+} pathways to induce its full transcriptional effect. Thus, PMA effects appeared in keeping with a cross-talk between PKC and Ca^{2+} pathways during megakaryocytic-erythroid differentiation.[2,30]

Table 2 Differential expression of transcriptional regulators in Meg-01-*GRIN1*$^{-/-}$ cells compared with unmodified Meg-01 cells determined from Clariom S microarrays

Gene name	Transcription factor/regulator	Fold change	*p*-Value	FDR
HEY1	Hes related family basic helix-loop-helix transcription factor with YRPW motif 1	16.65	1.36E-11	4.84E-08
ZEB1	Zinc finger E-box binding homeobox 1	16.42	5.24E-12	4.84E-8
JUN	Jun proto-oncogene	3.47	5.21E-06	3.00E-04
ID1	Inhibitor of DNA binding 1	3.16	7.88E-09	3.02E-06
ID3	Inhibitor of DNA binding 2	3.03	2.29E-05	9.00E-04
EGR1	Early growth response 1	2.67	4.80E-07	5.32E-05
HEY2	Hes related family BHLH transcription factor with YRPW motif 2	2.27	7.69E-07	7.63E-05
PAX6	Paired box 6	2.28	0.0141	0.0926
KLF3	Kruppel like factor 3	1.93	4.24E-05	1.40E-03
KLF6	Kruppel like factor 6	1.72	2.47E-05	9.00E-04
CREBRF	CREB3 regulatory factor	1.68	7.96E-05	0.0023
NFATC1	Nuclear factor of activated T-cells, cytoplasmic, calcineurin-dependent 1	1.7	6.76E-05	0.0020
KLF1	Kruppel like factor 1	1.57	9.12E-05	2.50E-03
KLF10	Kruppel like factor 10	1.56	1.00E-04	2.80E-03
ERG	ETS transcription factor ERG	−1.67	2.70E-06	2.00E-04
FLI1	FLI-1 proto-oncogene	−1.83	9.98E-07	9.27E-05
RUNX1	Runt related transcription factor 1	−1.85	1.57E-06	1.00E-04
MEIS1	Meis homeobox 1	−1.98	3.43E-06	0.0002

Abbreviation: FDR, false discovery rate.

Memantine Increases Cytarabine-Mediated Cell Killing of Meg-01 Cells

The increased levels of cytoplasmic Ca^{2+}, ER stress response, autophagy induction, and higher LDH release suggested that Meg-01-*GRIN1*$^{-/-}$ cells had a lower threshold for cell death. We hypothesized this pro-death state would make cells more vulnerable to additional toxic insults, and tested if NMDAR inhibition would increase cell killing by cytarabine (currently, a cornerstone of antileukemia treatment). Memantine was employed in these experiments, as it is an approved drug used in neurological patients. Meg-01 cells were pretreated with 100 µM memantine for 1 hour, followed by 3 days with 0.1 µM (low dose) cytarabine; effects on cell numbers were tested using an MTT assay (►**Fig. 7**). Even this brief exposure to memantine resulted in 3.1-times more cell killing compared with cytarabine alone (►**Fig. 7**).

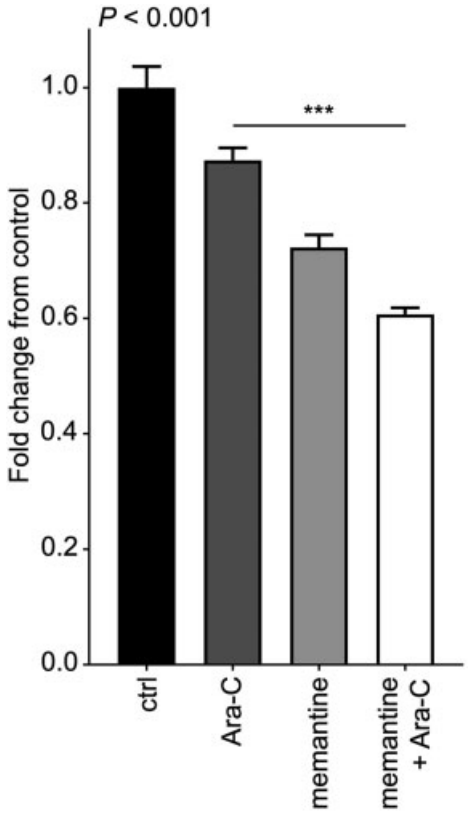

Fig. 7 Effect of memantine on cytarabine-induced cell killing of Meg-01 cells. Meg-01 cells were pretreated with memantine 100 µM for 1 hour and then cultured with cytarabine (Ara-C; 100 nm) for 3 days. Cell viability was measured by MTT assay. Bars are mean ± standard error of the mean from four independent experiments each in triplicate. Statistical significance is shown (one-way ANOVA with Dunnet *post hoc*; $^{***}p < 0.001$). Ara-C, cytarabine; ctrl, control; MTT, 3-(4,5-dimethylthiazol-2-yl)-2,5-diphenyltetrazolium bromide.

Discussion

This study provides the first evidence that NMDARs comprise an integral component of the Ca^{2+} toolkit in Meg-01 cells, with NMDAR function required to prevent cell stress and support megakaryocytic over erythroid differentiation.

CRISPR-Cas9-mediated NMDAR hypofunction caused marked changes in Ca^{2+} homeostasis in Meg-01 cells, resulting in atypical differentiation, basal ER stress and cell death. Meg-01-*GRIN1*$^{-/-}$ cells accumulated lysosome-related organelles, suggesting abnormalities in membrane trafficking. Resting cytosolic Ca^{2+} levels were higher in Meg-01-*GRIN1*$^{-/-}$ cells, but ER Ca^{2+} release and SOCE were lower after activation. *GRIN1* deletion affected the transcription of the following Ca^{2+} toolkit genes: *TRPC6*, *CACNA1A*, *MCOLN3*, *ATP2A3*, *ATP2B4*, *SLC24A3*, *CALN1*, *CALB1* and *SCIN*; most of which also changed in response to memantine. Increased levels of *JUN*, *DDIT3*, *ATF4*, *PPP1R15A* and *XBP1* spliced transcripts indicated ER stress, and a shift in megakaryocytic-erythroid transcription factors explained features of erythroid differentiation. Finally, pharmacologic NMDAR inhibition using memantine increased cell killing by cytarabine.

Despite increasing evidence that pharmacologic NMDAR inhibitors disturb megakaryocytic maturation,[8,10–12] NMDAR roles in MKs remained speculative. Our work adds solid evidence that NMDARs operate as important components of the Ca^{2+} toolkit in Meg-01 cells; hence, further analysis in normal and malignant MKs may uncover meaningful NMDAR roles. Similar to the NMDAR, several other components of the Ca^{2+} toolkit found differentially expressed in Meg-01-*GRIN1*$^{-/-}$ cells (e.g. *TRPC6*, *CACNA1A*, *MCOLN3*, *CALN1* and *CALB1*) are best known for their neuronal functions. Our results suggest that these molecules have previously unappreciated roles in megakaryocytic and erythroid differentiation.

Recent work provided computational support for the NMDAR involvement in human erythropoiesis. The *GRIN3B* gene, encoding the GluN3B subunit of NMDAR, has been linked with signaling through ErbB4 (epidermal growth factor receptor Erb-B2 receptor tyrosine kinase 4), which balances erythropoiesis against other myeloid lineages (in particular megakaryopoiesis) in multiple *in vivo* and *ex vivo* models.[31] Our results are consistent with these data. Using Meg-01 cell line that carries dual, megakaryocytic-erythroid differentiation potential, we provide the first experimental evidence that NMDARs and intracellular Ca^{2+} homeostasis balance megakaryocytic and erythroid cell fates.

Differentiation of megakaryocytic and erythroid lineages are closely connected and regulated by a set of transcription factors that include *RUNX1*, *ERG*, *FLI1*, *GATA* and *KLF* family members.[32] RUNX1 increases megakaryocytic and represses erythroid differentiation by antagonising the erythroid master regulator KLF1.[33] The converse is also true, as KLF1 inhibits megakaryopoiesis.[34] We found that *KLF1*, *KLF3*, *KLF6* and *KLF10* were expressed to higher levels in Meg-01-*GRIN1*$^{-/-}$ cells, *GATA1* and *GATA2* were unchanged, and *RUNX1*, *FLI1*, *ERG* and *MEIS1* were expressed to lower levels compared with control Meg-01 cells, consistent with the phenotypic bias toward erythropoiesis detected in Meg-01-*GRIN1*$^{-/-}$ cells. Based on CD41 and CD235a expression, Meg-01-*GRIN1*$^{-/-}$ cells were heterogeneous (including erythroid, megakaryocytic, and double-positive cells; ►**Supplementary Fig. S12Bii**, available in the online version) that may explain the discrepancy between their higher ploidy and lower CD41/CD61 expression for the overall population.

We do not know what mechanisms were responsible for transcription factor alterations in Meg-01-*GRIN1*$^{-/-}$ cells. Microarray analysis showed *NFATC1* transcript levels were higher (►**Table 2**), but there was no transcriptional signature of enhanced NFAT activity (data not shown). Other pathways through which NMDARs regulate transcription include calcium / calmodulin-dependent protein kinases (CaMK).[35] Expression of *CAMKIV* was reduced in Meg-01-*GRIN1*$^{-/-}$ cells (FC -1.91; **Supplementary Microarray Excel Data File**, available in the online version), raising the possibility that this pathway is operational in MKs, but functional validation is required.

This is not the first study to report that a membranous Ca^{2+} channel affects the balance of megakaryocytic-erythroid differentiation. Overexpression of TRPA1 (ankyrin 1; a TRPC family channel that contributes to SOCE in Meg-01 cells[36]) was shown to suppress erythroid but enhance megakaryocytic differentiation in K-562 and HEL cell lines; however, the mechanism of TRPA1 action was not examined in that study.[37] Our findings are in agreement, showing the reciprocal effect, as reduced NMDAR function enhances erythroid differentiation. Therefore, similar to TRPA1, normal NMDAR activity favors megakaryocytic differentiation. Previous authors suggested therapeutic opportunities involving modulation of TRPA1 in disorders associated with anemia and thrombocytopenia.[37] Our results suggest that NMDAR (and possibly other components of the Ca^{2+} toolkit) may provide similar opportunities. As a proof of principle, we show that memantine, a drug used to treat neurological patients, increases Meg-01 cell killing by cytarabine, suggesting a drug combination for further testing in primary cells.

Based on what is known about normal functions of the Ca^{2+} toolkit genes, we propose the following changes compensated for the NMDAR hypofunction in Meg-01 cells (►**Fig. 8**). Reduced expression of *TRPC6* and *CANA1A* restricted Ca^{2+} influx across the plasma membrane. Lower levels of *ATP2A3* and *CALN1* transcripts reduced ER Ca^{2+} stores,[38] implying that overall Meg-01-*GRIN1*$^{-/-}$ cells experienced a form of Ca^{2+} "starvation." However, resting Ca^{2+} levels were higher in Meg-01-*GRIN1*$^{-/-}$ cells, suggesting an alternative mechanism to increase cytosolic Ca^{2+} levels. Higher expression of *MCOLN3* may contribute Ca^{2+} efflux from immature lysosomal organelles that accumulated in Meg-01-*GRIN1*$^{-/-}$ cells.[39] In support, glutamate recruits lysosomal Ca^{2+} stores in neurons and glia.[40] In addition, lower levels of *ATP2A3*, *ATP2B4* and *SLC24A3* transcripts may reduce exclusion of cytosolic Ca^{2+} into the ER and the extracellular compartment, respectively. Increased cytosolic Ca^{2+} levels observed in Meg-01-*GRIN1*$^{-/-}$ cells were likely required to preserve signaling, but also implied a stressed, pro-apoptotic cell state. It is possible that higher expression of *CALB1* rescued Meg-01-*GRIN1*$^{-/-}$ cells from apoptosis,[41,42] and *SCIN* contributed to differentiation.[43] Overall, the range of transcriptomic changes we found in Meg-01-*GRIN1*$^{-/-}$ cells indicate that NMDARs work together with other Ca^{2+} channels, such as TRPC6, Cav2.1 and TRPML3 located in the plasma and lysosomal membranes respectively, to support Ca^{2+} signaling in Meg-01 cells (►**Fig. 8**).

The increase in lysosomal organelles and associated *MCOLN3* upregulation in Meg-01-*GRIN1*$^{-/-}$ cells are intriguing. Lysosomes and platelet dense granules share

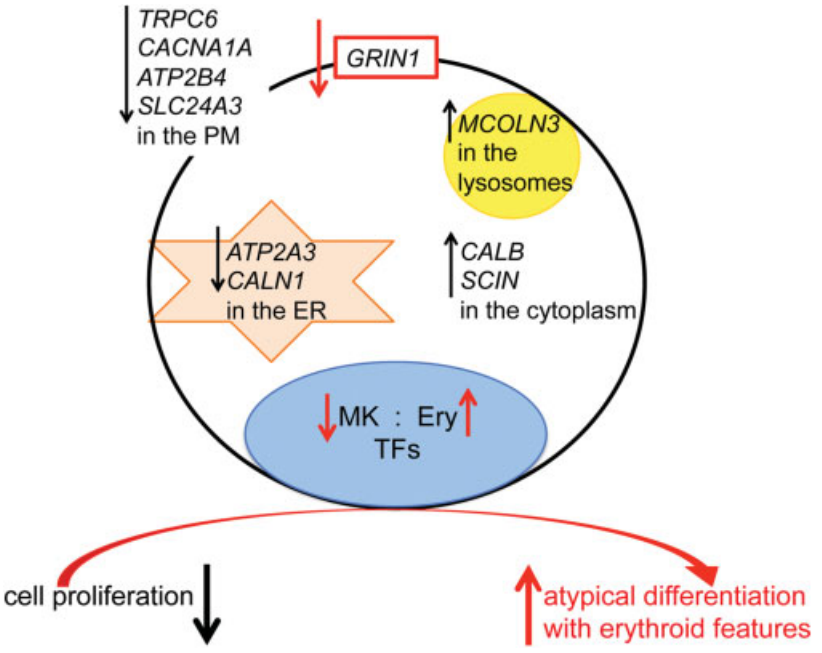

Fig. 8 Schematic summary of the changes caused by *GRIN1* deletion in Meg-01 cells. *GRIN1* deletion in Meg-01 cells induced NMDAR hypofunction that led to the significant remodeling of the Ca^{2+} regulatory network associated with atypical differentiation showing erythroid features. Reduced expression of *TRPC6* and *CACNA1A* had the potential to reduce Ca^{2+} entry from the extracellular environment. Lower levels of *ATP2A3* and *CALN1* could reduce ER Ca^{2+} stores, leading to ER stress. Lower levels of *ATP2A3*, *ATP2B4* and *SLC24A3*, and higher levels of *MCOLN3* had the potential to increase cytoplasmic Ca^{2+} levels, buffered by increased expression of *CALB1*. Higher levels of *SCIN* could assist differentiation. *GRIN1* deletion also altered expression of selected hematopoietic transcription factors, demonstrating a decrease in megakaryocytic but an increase in erythroid regulators, in keeping with increased erythroid differentiation of Meg-01-*GRIN1*$^{-/-}$ cells. The subcellular sites of expression indicated on the schematic apply to the proteins encoded by the genes shown. ER, endoplasmic reticulum; Ery, erythroid; MK, megakaryocytic; PM, plasma membrane; TF, transcription factor.

biogenesis[44,45] and secretion mechanisms.[46] TRPML3 is expressed in early lysosomes where it regulates Ca^{2+} efflux and related membrane trafficking.[39] Our evidence for increased lysosomal and ER accumulation in Meg-01-*GRIN1*$^{-/-}$ cells corroborates previous findings by our group and others of increased cytoplasmic vacuolation arising in megakaryocytic cells in the presence of NMDAR inhibitors.[10–12] To our knowledge, this is the first study to report potential NMDAR contribution to lysosomal biogenesis in megakaryocytic cells.

Our study has several limitations. The phenotype of Meg-01-*GRIN1*$^{-/-}$ cells may be contributed by other mechanisms that occurred downstream or independently of reduced Ca^{2+} influx through the NMDAR. We did not dissect the roles of individual molecular changes we found, and cannot depict NMDAR pathways in megakaryocytic cells. Our results raise the possibility that NMDARs regulate Ca^{2+} storage/release from the lysosomal organelles, but no measurements of lysosomal Ca^{2+} were performed. Our conclusions are derived from studies in one, one cell line. Meg-01 cells were chosen based on our previous findings showing that they are better suited than K-562 and Set-2 cells to study NMDAR function. However, more detailed characterization of the Ca^{2+} toolkit is required using other models of megakaryocytic and erythroid differentiation. Examination of the Ca^{2+} toolkit may also be rewarding in myeloproliferative neoplasms, as *CALR* gene mutations are predicted to reduce Ca^{2+} binding in the ER,[47] which could trigger ER stress, recently revealed in patient cells.[48]

In summary, CRISPR-Cas9-mediated *GRIN1* deletion disturbed Ca^{2+} homeostasis in Meg-01 cells and shifted differentiation toward the erythroid lineage. The downstream effects of the reduced NMDAR function involved changes in ER Ca^{2+} release, lysosome-related organelles, Ca^{2+} toolkit molecules, and megakaryocytic-erythroid transcription factors. Our findings strengthen the evidence for the importance of NMDAR and intracellular Ca^{2+} homeostasis in megakaryocytic cell function, including balancing of ER stress and megakaryocytic-erythroid differentiation.

What is known about this topic?

- Intracellular signaling by calcium ions (Ca^{2+}) supports differentiation of normal megakaryocytes.
- *N*-methyl-D-aspartate receptors (NMDARs) appear to operate as Ca^{2+} channels in megakaryocytic cells.

What does this paper add?

- We provide the first genetic evidence that NMDARs are an integral component of the Ca^{2+} toolkit in megakaryocytic cells.
- NMDARs favor megakaryocytic over erythroid differentiation, support dense granule biogenesis, and contribute to Ca^{2+} homeostasis in the endoplasmic reticulum.
- Modulation of Ca^{2+} homeostasis offers potential to inhibit proliferation of malignant megakaryocytes and increase erythroid differentiation.

Authors' Contributions

M.L.K.Z designed the study. J.I.H., T.N.G., M.C., Y.N.S.N., L.L. and M.L.K.Z generated and analysed data. N.C., C.B., R.C.P., D.C.S., S.K.B. and M.L.K.Z provided methodology advice, supervision and mentorship. J.I.H., T.N.G. and M.L.K.Z wrote the manuscript. All authors edited the manuscript and approved the final version for submission.

Note

J.I.H. received PhD scholarship from Anne and Victoria Norman, supplemented by payments from the Marijana Kumerich Trust.

Funding

This work was funded by Auckland Medical Research Foundation, Leukemia & Blood Cancer New Zealand, and Cancer Research Trust.

Conflict of Interest

None declared.

Acknowledgments

Jacqueline Ross and Hilary Holloway (Biomedical Imaging Research Unit) helped with electron microscopy. Stephen Edgar (Molecular Medicine and Pathology) and Michelle Petrasich (LabPlus) supported flow cytometry work. Liam Williams (New Zealand Genomics Limited) processed Clariom S microarrays. We are grateful to Dr Elizabeth Ledgerwood for helpful discussions and comments on the manuscript.

References

1 Berridge MJ, Bootman MD, Roderick HL. Calcium signalling: dynamics, homeostasis and remodelling. Nat Rev Mol Cell Biol 2003;04(07):517–529
2 Di Buduo CA, Balduini A, Moccia F. Pathophysiological significance of store-operated calcium entry in megakaryocyte function: opening new paths for understanding the role of calcium in thrombopoiesis. Int J Mol Sci 2016;17(12):17
3 Berridge MJ. Inositol trisphosphate and calcium signalling mechanisms. Biochim Biophys Acta 2009;1793(06):933–940
4 Clapham DE. Calcium signaling. Cell 2007;131(06):1047–1058
5 Zaslavsky A, Chou ST, Schadler K, et al. The calcineurin-NFAT pathway negatively regulates megakaryopoiesis. Blood 2013;121 (16):3205–3215
6 Di Buduo CA, Moccia F, Battiston M, et al. The importance of calcium in the regulation of megakaryocyte function. Haematologica 2014;99(04):769–778
7 Wang JX, Furukawa H. Dissecting diverse functions of NMDA receptors by structural biology. Curr Opin Struct Biol 2019; 54:34–42
8 Genever PG, Wilkinson DJ, Patton AJ, et al. Expression of a functional N-methyl-D-aspartate-type glutamate receptor by bone marrow megakaryocytes. Blood 1999;93(09):2876–2883
9 Traynelis SF, Wollmuth LP, McBain CJ, et al. Glutamate receptor ion channels: structure, regulation, and function. Pharmacol Rev 2010;62(03):405–496
10 Kamal T, Green TN, Morel-Kopp MC, et al. Inhibition of glutamate regulated calcium entry into leukemic megakaryoblasts reduces cell proliferation and supports differentiation. Cell Signal 2015;27 (09):1860–1872

11 Kamal T, Green TN, Hearn JI, et al. *N*-methyl-d-aspartate receptor mediated calcium influx supports in vitro differentiation of normal mouse megakaryocytes but proliferation of leukemic cell lines. Res Pract Thromb Haemost 2017;02(01):125–138
12 Hitchcock IS, Skerry TM, Howard MR, Genever PG. NMDA receptor-mediated regulation of human megakaryocytopoiesis. Blood 2003;102(04):1254–1259
13 Ogura M, Morishima Y, Ohno R, et al. Establishment of a novel human megakaryoblastic leukemia cell line, MEG-01, with positive Philadelphia chromosome. Blood 1985;66(06): 1384–1392
14 Ogura M, Morishima Y, Okumura M, et al. Functional and morphological differentiation induction of a human megakaryoblastic leukemia cell line (MEG-01s) by phorbol diesters. Blood 1988; 72(01):49–60
15 Trécul A, Morceau F, Gaigneaux A, Schnekenburger M, Dicato M, Diederich M. Valproic acid regulates erythro-megakaryocytic differentiation through the modulation of transcription factors and microRNA regulatory micro-networks. Biochem Pharmacol 2014;92(02):299–311
16 Chen W, Arroyo JD, Timmons JC, Possemato R, Hahn WC. Cancer-associated PP2A Aalpha subunits induce functional haploinsufficiency and tumorigenicity. Cancer Res 2005;65(18): 8183–8192
17 Kalev-Zylinska ML, Hearn JI, Rong J, et al. Altered N-methyl D-aspartate receptor subunit expression causes changes to the circadian clock and cell phenotype in osteoarthritic chondrocytes. Osteoarthritis Cartilage 2018;26(11):1518–1530
18 Kalev-Zylinska ML, Green TN, Morel-Kopp MC, et al. N-methyl-D-aspartate receptors amplify activation and aggregation of human platelets. Thromb Res 2014;133(05):837–847
19 Livak KJ, Schmittgen TD. Analysis of relative gene expression data using real-time quantitative PCR and the 2(-Delta Delta C(T)) Method. Methods 2001;25(04):402–408
20 van Galen P, Kreso A, Mbong N, et al. The unfolded protein response governs integrity of the haematopoietic stem-cell pool during stress. Nature 2014;510(7504):268–272
21 Lasham A, Herbert M, Coppieters 't Wallant N, et al. A rapid and sensitive method to detect siRNA-mediated mRNA cleavage in vivo using 5′ RACE and a molecular beacon probe. Nucleic Acids Res 2010;38(03):e19
22 Singleton DC, Rouhi P, Zois CE, et al. Hypoxic regulation of RIOK3 is a major mechanism for cancer cell invasion and metastasis. Oncogene 2015;34(36):4713–4722
23 Irizarry RA, Hobbs B, Collin F, et al. Exploration, normalization, and summaries of high density oligonucleotide array probe level data. Biostatistics 2003;04(02):249–264
24 Ambrosio AL, Boyle JA, Di Pietro SM. Mechanism of platelet dense granule biogenesis: study of cargo transport and function of Rab32 and Rab38 in a model system. Blood 2012;120(19): 4072–4081
25 Pérez-Riesgo E, Gutiérrez LG, Ubierna D, et al. Transcriptomic analysis of calcium remodeling in colorectal cancer. Int J Mol Sci 2017;18(05):18
26 Ramanathan G, Mannhalter C. Increased expression of transient receptor potential canonical 6 (TRPC6) in differentiating human megakaryocytes. Cell Biol Int 2016;40(02):223–231
27 Kaestner L, Wang X, Hertz L, Bernhardt I. Voltage-activated ion channels in non-excitable cells-a viewpoint regarding their physiological justification. Front Physiol 2018;09:450
28 Zhao P, Xiao X, Kim AS, et al. c-Jun inhibits thapsigargin-induced ER stress through up-regulation of DSCR1/Adapt78. Exp Biol Med (Maywood) 2008;233(10):1289–1300
29 Isakari Y, Sogo S, Ishida T, et al. Gene expression analysis during platelet-like particle production in phorbol myristate acetate-treated MEG-01 cells. Biol Pharm Bull 2009;32(03):354–358
30 Brignall R, Cauchy P, Bevington SL, et al. Integration of kinase and calcium signaling at the level of chromatin underlies inducible gene activation in T cells. J Immunol 2017;199(08):2652–2667
31 Kinney MA, Vo LT, Frame JM, et al. A systems biology pipeline identifies regulatory networks for stem cell engineering. Nat Biotechnol 2019;37(07):810–818
32 Zhu F, Feng M, Sinha R, Seita J, Mori Y, Weissman IL. Screening for genes that regulate the differentiation of human megakaryocytic lineage cells. Proc Natl Acad Sci U S A 2018;115(40):E9308–E9316
33 Kuvardina ON, Herglotz J, Kolodziej S, et al. RUNX1 represses the erythroid gene expression program during megakaryocytic differentiation. Blood 2015;125(23):3570–3579
34 Frontelo P, Manwani D, Galdass M, et al. Novel role for EKLF in megakaryocyte lineage commitment. Blood 2007;110(12): 3871–3880
35 Cohen S, Greenberg ME. Communication between the synapse and the nucleus in neuronal development, plasticity, and disease. Annu Rev Cell Dev Biol 2008;24:183–209
36 Albarrán L, Lopez JJ, Dionisio N, Smani T, Salido GM, Rosado JA. Transient receptor potential ankyrin-1 (TRPA1) modulates store-operated Ca(2+) entry by regulation of STIM1-Orai1 association. Biochim Biophys Acta 2013;1833(12):3025–3034
37 Chen JL, Ping YH, Tseng MJ, et al. Notch1-promoted TRPA1 expression in erythroleukemic cells suppresses erythroid but enhances megakaryocyte differentiation. Sci Rep 2017;07:42883
38 Kobuke K, Oki K, Gomez-Sanchez CE, et al. Calneuron 1 increased Ca(2+) in the endoplasmic reticulum and aldosterone production in aldosterone-producing adenoma. Hypertension 2018;71(01): 125–133
39 Kim HJ, Soyombo AA, Tjon-Kon-Sang S, So I, Muallem S. The Ca (2+) channel TRPML3 regulates membrane trafficking and autophagy. Traffic 2009;10(08):1157–1167
40 Pandey V, Chuang CC, Lewis AM, et al. Recruitment of NAADP-sensitive acidic Ca2+ stores by glutamate. Biochem J 2009;422 (03):503–512
41 Kook SY, Jeong H, Kang MJ, et al. Crucial role of calbindin-D28k in the pathogenesis of Alzheimer's disease mouse model. Cell Death Differ 2014;21(10):1575–1587
42 Bellido T, Huening M, Raval-Pandya M, Manolagas SC, Christakos S. Calbindin-D28k is expressed in osteoblastic cells and suppresses their apoptosis by inhibiting caspase-3 activity. J Biol Chem 2000;275(34):26328–26332
43 Zunino R, Li Q, Rosé SD, et al. Expression of scinderin in megakaryoblastic leukemia cells induces differentiation, maturation, and apoptosis with release of plateletlike particles and inhibits proliferation and tumorigenesis. Blood 2001;98(07):2210–2219
44 Polasek J. Platelet secretory granules or secretory lysosomes? Platelets 2005;16(08):500–501
45 Ambrosio AL, Di Pietro SM. Storage pool diseases illuminate platelet dense granule biogenesis. Platelets 2017;28(02):138–146
46 Ambrosio AL, Boyle JA, Di Pietro SM. TPC2 mediates new mechanisms of platelet dense granule membrane dynamics through regulation of Ca2+ release. Mol Biol Cell 2015;26(18):3263–3274
47 Shivarov V, Ivanova M, Tiu RV. Mutated calreticulin retains structurally disordered C terminus that cannot bind Ca(2+): some mechanistic and therapeutic implications. Blood Cancer J 2014;04:e185
48 Nam AS, Kim KT, Chaligne R, et al. Somatic mutations and cell identity linked by Genotyping of Transcriptomes. Nature 2019; 571(7765):355–360